JURNAL KIMIA VALENSI
p-ISSN: 2460-6065; e-ISSN: 2548-3013
Journal homepage: https://journal.uinjkt.ac.id/index.php/valensi
Research Article

Molten Salt Synthesis of the Plate-Like ABi$_4$Ti$_4$O$_{15}$ (A= Ba, and Pb) for Methylene Blue Removal via Phocatalysis Effect

Anton Prasetyo[1*], Muhammad Lathif Al-Abror[1], Usman Ali Rouf[1], Erna Hastuti[2], Widiya Nur Safitri[3], Arie Hardian[4, 5]

[1]*Department of Chemistry, Faculty of Science and Technology, Universitas Islam Negeri Maulana Malik Ibrahim Malang, Jalan Gajayana 50, Malang, 65144, Indonesia*
[2]*Department of Physics, Faculty of Science and Technology, Universitas Islam Negeri Maulana Malik Ibrahim Malang, Jalan Gajayana 50, Malang, 65144, Indonesia*
[3]*Department of Chemistry, Faculty of Science and Data Analytics, Institut Teknologi Sepuluh Nopember, Keputih, Sukolilo, Surabaya, 60111, East Java, Indonesia*
[4]*Department of Chemistry, Faculty of Sciences and Informatics, Universitas Jenderal Achmad Yani, Cimahi, 40531, Indonesia*
[5]*Material and Environmental Development Center, Universitas Jenderal Achmad Yani, Cimahi, 40531, Indonesia*

[*]*Email: anton@kim.uin-malang.ac.id*

Article Info
Received: Nov 17, 2025
Revised: Apr 10, 2026
Accepted: Apr 18, 2026
Online: May 31, 2026

Citation:
Prasetyo, A., Al-Abror, M. L. Rouf, U. A., Hastuti, E., Safitri, W. N., Hardian, A. (2026). Molten Salt Synthesis of the Plate-Like ABi$_4$Ti$_4$O$_{15}$ (A= Ba, and Pb) for Methylene Blue Removal via Phocatalysis Effect. *Jurnal Kimia Valensi*, 12(1), 64-73.

Doi: 10.15408/jkv.v12i1.48900

Abstract

One of the promising technologies for the treatment of dye-containing wastewater is photocatalysis. Among the compounds reported to exhibit good photocatalytic activity are Aurivillius compounds with plate-like morphology. In this study, the plate-like ABi$_4$Ti$_4$O$_{15}$ (A= Ba and Pb) compounds was synthesized using the molten salt method. Diffractogram confirmed that the target compounds BaBi$_4$Ti$_4$O$_{15}$ and PbBi$_4$Ti$_4$O$_{15}$ were successfully synthesized but still found the impurities compound. And also the differences in the type of A-site cation (Ba and Pb) also affect the local structure, meanwhile, the SEM image showed that the particle morphology of all samples is plate-like, however, the particle size obtained is not uniform and agglomerated. The plot tauc calculations showed that BaBi$_4$Ti$_4$O$_{15}$ has a band gap energy of 3.28 eV (378 nm), while that of PbBi$_4$Ti$_4$O$_{15}$ is 3.03 eV (409.19 nm). Differences in the type of A-site cation (Ba and Pb) affect the band gap energy of the four-layer Aurivillius compound ABi$_4$Ti$_4$O$_{15}$. Then the lower band gap energy of PbBi$_4$Ti$_4$O$_{15}$ results in a higher degradation capability toward methylene blue compared to BaBi$_4$Ti$_4$O$_{15}$. It also related to higher reaction rate constant of PbBi$_4$Ti$_4$O$_{15}$. In addition, the another factor also influences the yield of methylene blue degradation by PbBi$_4$Ti$_4$O$_{15}$ is its higher adsorption ability.

Keywords: ABi$_4$Ti$_4$O$_{15}$ (A= Ba and Pb), molten salt synthesis, methylene blue, photocatalysis

1. INTRODUCTION

Methylene blue is a synthetic dye used by the textile industry and produced waste that seriously threatens the environmental ecosystem because methylene blue is toxic, carcinogenic, and environmentally persistent [1–3]. Therefore, developing methods for handling methylene blue waste has become important. One potential method for removing methylene blue is photocatalysis which can degrade organic compounds into smaller molecules, with CO_2 and H_2O as the end products and also have many advantages over other methods [4–6]. The photocatalysis method is a technique that utilizes light with energy greater than the band gap, and causing electrons in the valence band (*VB*) to be excited and transition to the conduction band (*CB*). In *VB*, holes (h^+) are formed, while electrons (e^-) are exist in *CB*. The presence of these h^+ and e^- species leads to the formation of •O and •OH radicals, which ultimately can degrade organic compounds [7,8]. The advantages of photocatalytic technology include: (a) it is environmentally friendly because it does not produce new waste, and (b) it is cost-effective since it can utilize sunlight as an energy source and the catalyst material can be reused [9,10].

One class of compounds reported to have potential as photocatalyst materials is the Aurivillius family of compounds [11,12]. Aurivillius compounds have the general formula $Bi_2O_2[A_{n-1}B_nO_{3n+1}]$, consisting of alternating bismuth layers and pseudo-perovskite layers along the *c*-axis. The *A* cation is +1, +2, or +3 charged cation with dodecahedral coordination, such as Na^+, Mg^{2+}, Sr^{2+}, Ba^{2+}, and Bi^{3+}. The *B* cation is a highly charged transition metal with octahedral coordination such as Nb^{5+}, Ti^{4+}, Ta^{6+}, V^{5+}, and W^{6+}, meanwhile "*n*" is an integer ($1 \leq n \leq 8$) that correlate to the number of octahedra in the perovskite layer [13]. One interesting property of Aurivillius compounds is their ferroelectric, which can inhibit the recombination rate of e^--h^+ pairs, thereby enhancing their photocatalytic activity [14,15]. In addition, compounds containing Bi atoms have been reported to exhibit good photocatalytic activity [16]. It indicated that Aurivillius compound family have the potential to be used in photocatalysis technology. Several Aurivillius compounds that have been used as photocatalyst materials include Bi_2WO_6, $BiMoO_6$, $Bi_4Ti_3O_{12}$, and $SrBi_4Ti_4O_{15}$ [17–20].

The compound $ABi_4Ti_4O_{15}$ (*A*= Ba and Pb) is classified as a member of the four-layer Aurivillius compound family. Qi *et al* reported that the compound $BaBi_4Ti_4O_{15}$ has a band gap energy of 3.2 eV and can degrade rhodamine B dye by 15% for 3.5 hours [21]. In addition, the compound $BaBi_4Ti_4O_{15}$ possesses good ferroelectric properties, which is advantageous when used as a photocatalytic material [22]. Kumar *et al* has reported that ferroelectric properties can enhance the photocatalytic activity of $BaBi_4Ti_4O_{15}$ in degrading methylene blue [22]. Meanwhile, the compound $PbBi_4Ti_4O_{15}$ has been reported to possess good spontaneous polarization and ferroelectricity [23]. Therefore, it has potency to use on photocatalyst technology. On other hand, the compound $PbBi_4Ti_4O_{15}$ has been reported to have a band gap energy of 3.15 eV [24]. However, its photocatalytic activity has not yet been reported. In addition, the type of *A*-site cation in perovskite-structured compounds is reported to influence photocatalytic properties due to differences in the size of the *A*-site cation, which affect the distortion of the octahedral structure [25,26]. However, studies on the photocatalytic properties of four-layer Aurivillius compounds with variations in *A*-site cations are still limited.

The Aurivillius compound particles with plate-like morphology have been reported to exhibit good photocatalytic activity [12,27–29]. Chen *et al* reported that the plate-like $Bi_4Ti_3O_{12}$ compound has high photocatalytic activity. It relates to plate-like $Bi_4Ti_3O_{12}$, which possesses many active sites on its surface and can inhibit the recombination rate of e^--h^+ [30]. One of the synthesis methods for Aurivillius compounds that has been reported to produce plate-like/sheet Aurivillius particle morphology is the molten salt method [31–33]. The synthesis of four-layer Aurivillius compounds $ABi_4Ti_4O_{15}$ (Ba and Pb) via molten salt method has been reported by several researchers, including (a) Nurcahyaningtyas and Prasetyo (2024), who synthesized $BaBi_4Ti_4O_{15}$, [34] and (b) Zulhadjri *et al*, who synthesized $PbBi_4Ti_4O_{15}$ [23]. In addition, they reported obtaining particles with plate-like morphology [23,34]. Therefore, in this study, we investigate the photocatalytic properties of four-layer Aurivillius compounds with different *A*-site cations ($ABi_4Ti_4O_{15}$ (*A*= Ba and Pb)) in degrading methylene blue.

2. RESEARCH METHODS

Materials

Bi_2O_3 (Himedia, 99% powder), TiO_2 (Sigma-Aldrich, 99% powder), $BaCO_3$ (Merck, 99.9% powder), PbO (Merck, 99% powder), NaCl (Merck, 99% powder), KCl (Merck, 99% powder), $AgNO_3$ (Merck, 99% powder), acetone (Merck), and aquades.

Synthesis

The synthesis of $ABi_4Ti_4O_{15}$ (*A* = Ba, and Pb) compounds was carried out using the molten salt method, and a mixture of NaCl/KCl salts with a molar ratio of 1:1 was used. The required precursors and salts were calculated stoichiometrically, based on a target compound weight of 3 grams. The first step in the synthesis involved mixing the precursors (Bi_2O_3, TiO_2, $BaCO_3$, PbO) and calcined at 700°C for 8 hours. In the next step, the sample was removed from the furnace and mixed with the NaCl/KCl salts in a molar ratio of target compound to salt of 1:7. The mixture of sample and salts was then calcined at 750°C for 8 hours, removed from the furnace, and ground again for 30 minutes. After that, the mixture of sample and salts was calcined again at 800°C for 8 hours. The calcination used a heating rate of 4 °C/min and cooled naturally. The resulting sample was taken from the furnace and washed with hot distilled water to take out the NaCl and KCl salt. The presence of residual NaCl and KCl salt in the sample was checked using $AgNO_3$. The salt-free product sample was then dried in an oven at 110°C for 3 hours.

Characterization

In this research, we used several characterization techniques: (a) *X*-ray diffraction (XRD) was used to identify the crystalline phases in the product sample. The analysis was carried out using a diffractometer (Rigaku Miniflex) with Cu Kα radiation (λ= 1.540593 Å), and measured at 2θ= 3-90°. (b) scanning electron microscopy (A JEOL JSM-6360LA) examined the particle morphology. (c)

ultraviolet-visible diffuse reflectance spectroscopy (Thermo Scientific Evolution 220) was used to determine the optical reflectance behavior of the samples. Then the data obtained were further analyzed using the Kubelka-Munk equation to determine the band gap energy. These measurements were performed using a Thermo Scientific Evolution 220 spectrometer over a 200-800 nm wavelength range.

Adsorption Test

The adsorption test was carried out at room temperature. Firstly, 4 ppm methylene blue and 0.1 gram of ABi$_4$Ti$_4$O$_{15}$ (A= Ba and Pb) were added to 100 mL of methylene blue and stirred in the dark condition for 30 minutes. Then, filtration was carried out to separate the filtrate from the adsorbent. And finally the remaining methylene blue in filtrate were measured using UV-Vis spectroscopy (Thermo Scientific Evolution 220).

Photocatalyst test

A 100 mL methylene blue with a concentration of 4 ppm and 0.1 grams of ABi$_4$Ti$_4$O$_{15}$ (A= Ba and Pb) was mixed. The resulting mixture was stirred in the dark condition for 30 minutes. Afterward, the suspension was exposed to ultraviolet light in a photoreactor equipped with eight Gaxindo T5 N093 UV lamps (Each lamp has an intensity of 119 lux), each rated at 8 watts, for 30, 60, 90, and 120 minutes. And then the remaining methylene blue concentration was measured using a UV-Vis spectrophotometer (Thermo Scientific Evolution 220)

3. RESULTS AND DISCUSSION

The diffractogram of the synthesized compound ABi$_4$Ti$_4$O$_{15}$ (A= Ba, and Pb) is shown in **Figure 1** and compared with standard data (Joint Committee on Powder Diffraction Standards/JCPDS No. 35-0757 for BaBi$_4$Ti$_4$O$_{15}$, and JCPDS No. 43-0972 for PbBi$_4$Ti$_4$O$_{15}$). The comparison results showed that the diffractogram of the target compounds matches the standard data that indicated the target compounds BaBi$_4$Ti$_4$O$_{15}$ and PbBi$_4$Ti$_4$O$_{15}$ were successfully synthesized. However, additional peaks were observed that indicated the impurity phases formed. In the BaBi$_4$Ti$_4$O$_{15}$ sample, an additional peak was found at 2θ= 31.7°, which corresponds to BaTiO$_3$, while in the PbBi$_4$Ti$_4$O$_{15}$ sample, an additional peak appeared at 2θ= 28.8°, corresponding to Bi$_2$Ti$_2$O$_7$. The very low intensity of the impurity peaks indicates that the concentration of these impurity compounds is very small, possibly due to incomplete grinding of the samples.

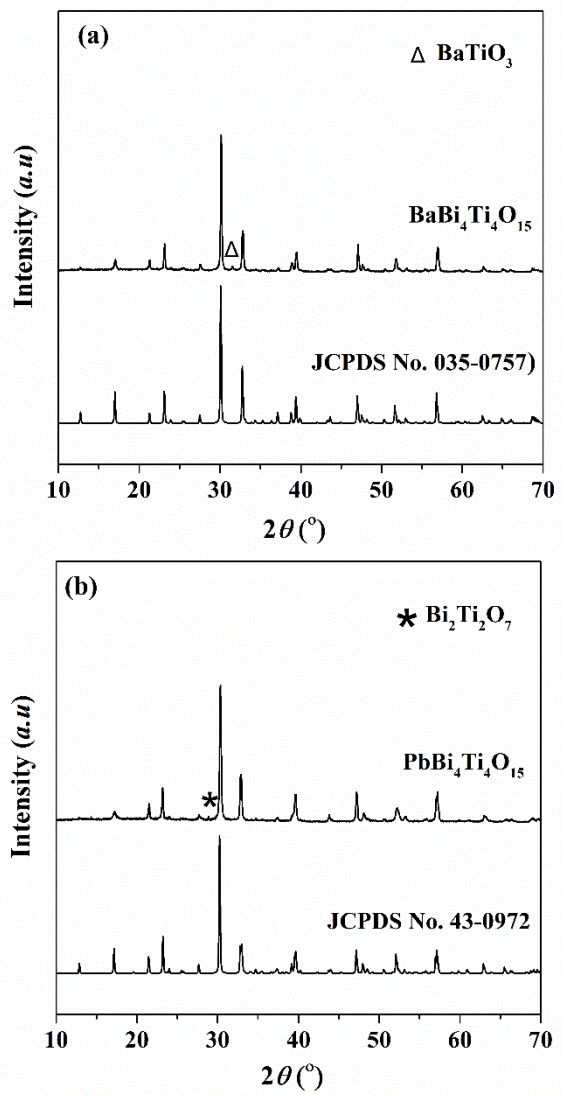

Figure 1. Diffractogram of ABi$_4$Ti$_4$O$_{15}$ (A= Ba, and Pb)

The phase identification and structural refinement of BaBi$_4$Ti$_4$O$_{15}$ and PbBi$_4$Ti$_4$O$_{15}$ ceramics were carried out using diffractogram processed with the Rietica software employing the Le Bail refinement method . This approach allows accurate extraction of lattice parameters and profile fitting without requiring a full structural model, making it suitable for complex layered oxide systems. **Figure 2** showed the refinement plot of sample diffractogram.

The refinement results (**Table 1**) indicate that BaBi$_4$Ti$_4$O$_{15}$ crystallizes predominantly in an orthorhombic structure with the space group $A2_1am$. The refined lattice parameters (a = 5.4522 Å, b = 5.4482 Å, and c = 41.733 Å) are consistent with the typical Aurivillius phase layered structure [18]. The high phase purity of BaBi$_4$Ti$_4$O$_{15}$ is evidenced by its dominant molar fraction of 98.71%, with only a minor secondary phase of BaTiO$_3$ (1.29%) detected. The relatively low R-factors (R_p = 9.93% and R_{wp} = 8.34%) confirm a good agreement between observed and calculated diffraction patterns, indicating a reliable refinement [35].

Table 1. Refinement data output

Sample	$BaBi_4Ti_4O_{15}$		$PbBi_4Ti_4O_{15}$	
	Phase 1	**Phase 2**	**Phase 1**	**Phase 2**
Crystal	$BaBi_4Ti_4O_{15}$	$BaTiO_3$	$PbBi_4Ti_4O_{15}$	$Bi_2Ti_2O_7$
Space Group	$A2_1am$	$P4mm$	$A2_1am$	Fd-$3m$
System Crystal	Orthorhombic	Tetragonal	Orthorhombic	Cubic
a (Å)	5.4522(4)	3.997(2)	5.4296(5)	10.380(1)
b (Å)	5.4482(6)	3.997(2)	5.4459(4)	10.380(1)
c (Å)	41.733(5)	4.040(4)	41.344(4)	10.380(1)
V (Å^3)	1239.7(2)	64.55(8)	1222.5(2)	1118.3(3)
Z	4	1	4	8
%molar	98.71(2)	1.29	35.34(1)	64.66(2)
R_p (%)	9.93		9.66	
R_{wp} (%)	8.34		7.25	

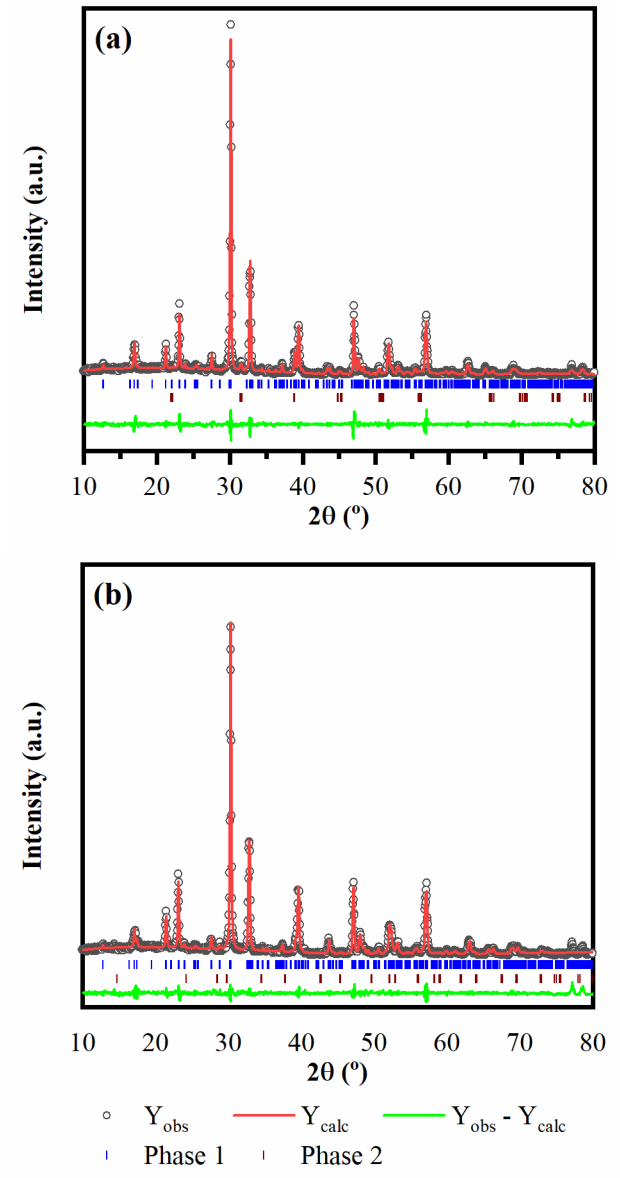

Figure 2. Refinement plot of Aurivillius structure of (a) $BaBi_4Ti_4O_{15}$ with secondary phase of $BaTiO_3$ and (b) $PbBi_4Ti_4O_{15}$ with secondary phase of $Bi_2Ti_2O_7$

In contrast, the $PbBi_4Ti_4O_{15}$ sample also adopts an orthorhombic structure with the same space group ($A2_1am$), but shows significantly different phase composition. The refined lattice parameters (a = 5.4296 Å, b = 5.4459 Å, and c = 41.344 Å) are slightly smaller than those of the Ba-based compound, reflecting the substitution effect of Pb^{2+} ions. However, the presence of a substantial secondary phase, identified as $Bi_2Ti_2O_7$ with a cubic structure (space group Fd-$3m$), dominates the sample with a molar fraction of 64.66%, while the main $PbBi_4Ti_4O_{15}$ phase constitutes only 35.34%. This suggests incomplete phase formation or phase instability in the Pb-containing system. Nevertheless, the refinement quality remains acceptable, as indicated by R_p = 9.66% and R_{wp} = 7.25%. The refinement plots (**Figure 2**) show good fitting between experimental and calculated patterns, with minimal residuals, further confirming the validity of the Le Bail fitting results. Regarding crystallite size, the average crystallite size was estimated from peak broadening analysis. The $BaBi_4Ti_4O_{15}$ sample exhibits a larger crystallite size of 43 ± 6 nm compared to $PbBi_4Ti_4O_{15}$, which has a smaller crystallite size of 33 ± 4 nm. This difference can be attributed to variations in ionic radius and diffusion behavior between Ba^{2+} (1.61 Å) and Pb^{2+} (1.39 Å) ions during the synthesis process. The smaller crystallite size in $PbBi_4Ti_4O_{15}$ may also be influenced by the presence of a significant secondary phase, which can hinder grain growth and promote structural disorder [36,37]. Overall, the analysis demonstrates that $BaBi_4Ti_4O_{15}$ achieves higher phase purity and larger crystallite size compared to $PbBi_4Ti_4O_{15}$. The substitution of Ba with Pb significantly affects phase formation, structural stability, and microstructural characteristics, which are critical factors for tailoring the functional properties of Aurivillius-type materials.

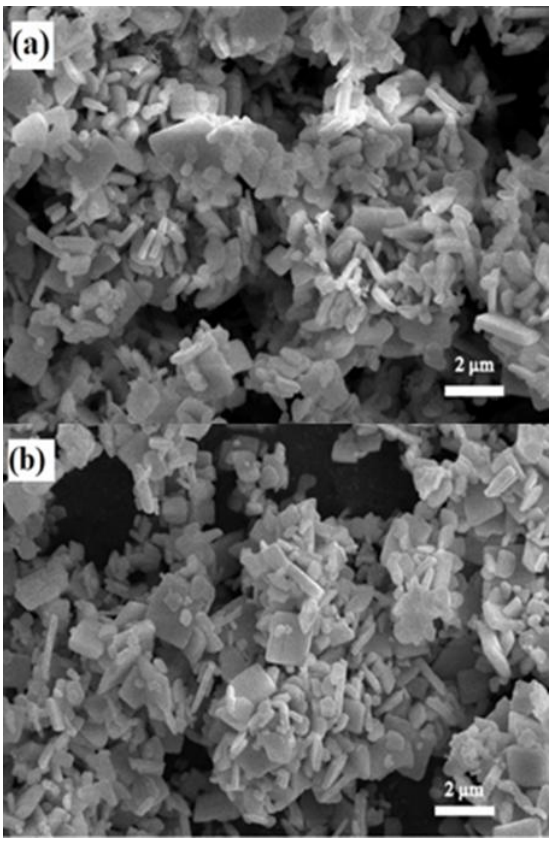

Figure 3. SEM image of ABi$_4$Ti$_4$O$_{15}$ (A= Ba, and Pb)

The SEM images of the ABi$_4$Ti$_4$O$_{15}$ compounds (A = Ba and Pb) are shown in **Figure 3**, and it can be seen that the particles exhibit a plate-like morphology, which is characteristic of Aurivillius-type structures [31,38]. **Figure 3** also shows that the BaBi$_4$Ti$_4$O$_{15}$ and PbBi$_4$Ti$_4$O$_{15}$ particles are stacked and agglomerated. It related to high synthesis temperatures used cause the particle agglomeration, and the faster ramp rate (the temperature increase from room temperature to the target temperature) is too rapid [39,40]. **Figure 3** also showed that the morphology of the two particles is not different. **Figure 4** showed the particle size distribution of ABi$_4$Ti$_4$O$_{15}$ (A= Ba and Pb) and can be seen that the BaBi$_4$Ti$_4$O$_{15}$ compound has a more uniform size compared to the PbBi$_4$Ti$_4$O$_{15}$ compound. It related to differences in particle growth rates and indicated that the PbBi$_4$Ti$_4$O$_{15}$ compound has a faster nucleation growth rate produce more number of particles [32,41].

The Tauc plot based on the Kubelka-Munk equation is shown in **Figure 5**, and the calculated band gap energies of ABi$_4$Ti$_4$O$_{15}$ (A = Ba, and Pb) are summarized in **Table 2**. It shows that the band gap energy of PbBi$_4$Ti$_4$O$_{15}$ is smaller than that of BaBi$_4$Ti$_4$O$_{15}$, which is related to the electronegativity value of the A-site cation. Hur *et al* reported that the A-site cation with higher electronegativity has a lower electron density, which weakens the bonding and decreases band gap energy (the Ba electronegativity is smaller than Pb). Their study also reported that a larger A-site cation decreases band gap energy due to the steric effect [42]. Meanwhile, the band gap energy of the ABi$_4$Ti$_4$O$_{15}$ (A = Ba, and Pb) compound involved electronic transitions from the Bi-6s and O-2p orbitals in the VB to the Ti-3d orbitals in the CB [43]. If compared with previously reported band gap energy measurements so it can be seen that the obtained value is slightly different [21,24]. This difference may be attributed to the presence of small amounts of impurity compounds.

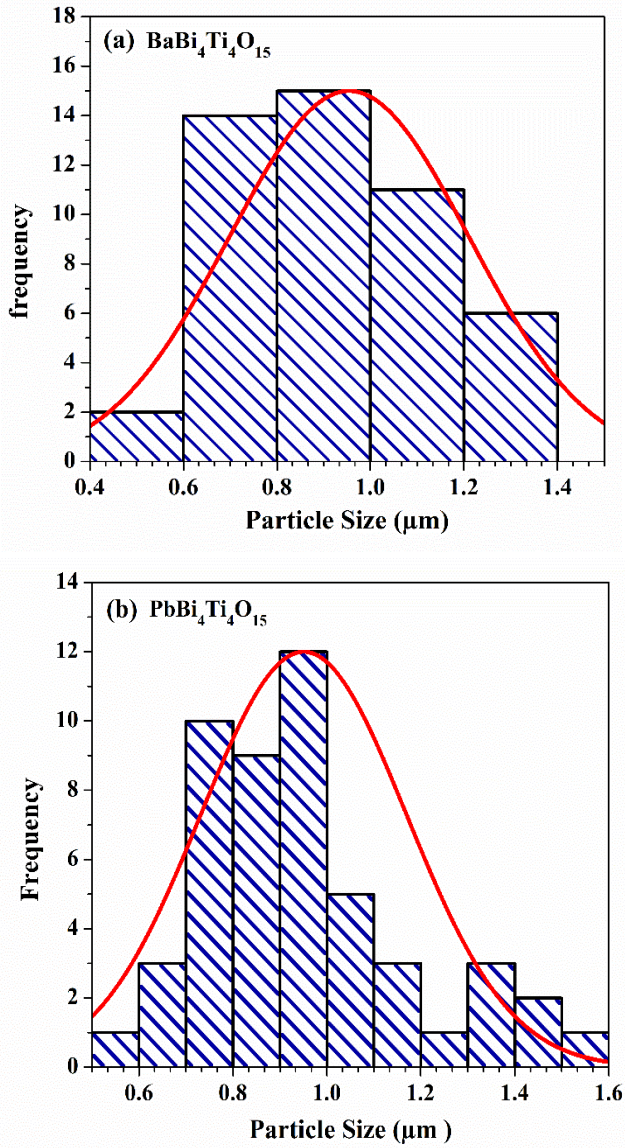

Figure 4. Particle size distribution of ABi$_4$Ti$_4$O$_{15}$ (A= Ba, and Pb)

The adsorption ability test result of the ABi$_4$Ti$_4$O$_{15}$ (A= Ba and Pb) compound is shown in **Figure 6**, and it can be seen that there is a decrease in absorbance value that correlates to reduction in methylene blue concentration (the results were summarized in **Table 3**). It showed that the ABi$_4$Ti$_4$O$_{15}$ (A= Ba and Pb) compound has adsorption capability, but it is not high. **Table 3** also shows that the adsorption ability of PbBi$_4$Ti$_4$O$_{15}$ is higher. It relates

to the particle size distribution calculation (**Figure 4**), which showed that the $PbBi_4Ti_4O_{15}$ material has many smaller particles. The adsorption properties of the four-layer Aurivillius compound has been reported by al Abrar *et al*, who reported that the $SrBi_4Ti_4O_{15}$ compound is capable of adsorbing methylene blue, although small [19]. The reports on the adsorption capability of Aurivillius compounds are still limited; therefore, there is no detailed mechanism of interaction between the adsorbate and Aurivillius compounds has been reported. However, if we are used to the model of Perovskite compounds, which have a similar structure so it may be that the dominant interaction is physisorption [44]. In addition, Huang *et al* suggested that the interaction mechanism in the methylene blue adsorption process with $PbTiO_3$ (one of the Perovskite compound) involves electrostatic interaction between the polarized property of the surface and the positive charge on the methylene blue molecules [45].

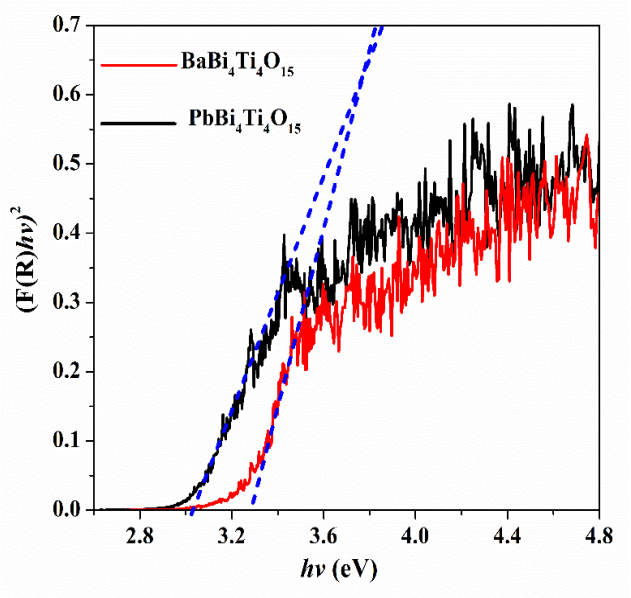

Figure 5. Tauc plot of ABi$_4$Ti$_4$O$_{15}$ (A= Ba, and Pb)

Table 2. The band gap energy of ABi$_4$Ti$_4$O$_{15}$ (A= Ba, and Pb)

Compound	Band gap energy (eV)
$BaBi_4Ti_4O_{15}$	3.28
$PbBi_4Ti_4O_{15}$	3.03

Table 3. The adsorption test results of ABi$_4$Ti$_4$O$_{15}$ (A= Ba, and Pb)

Compound	%Metylene blue concentration decreases
$BaBi_4Ti_4O_{15}$	6.25
$PbBi_4Ti_4O_{15}$	8.96

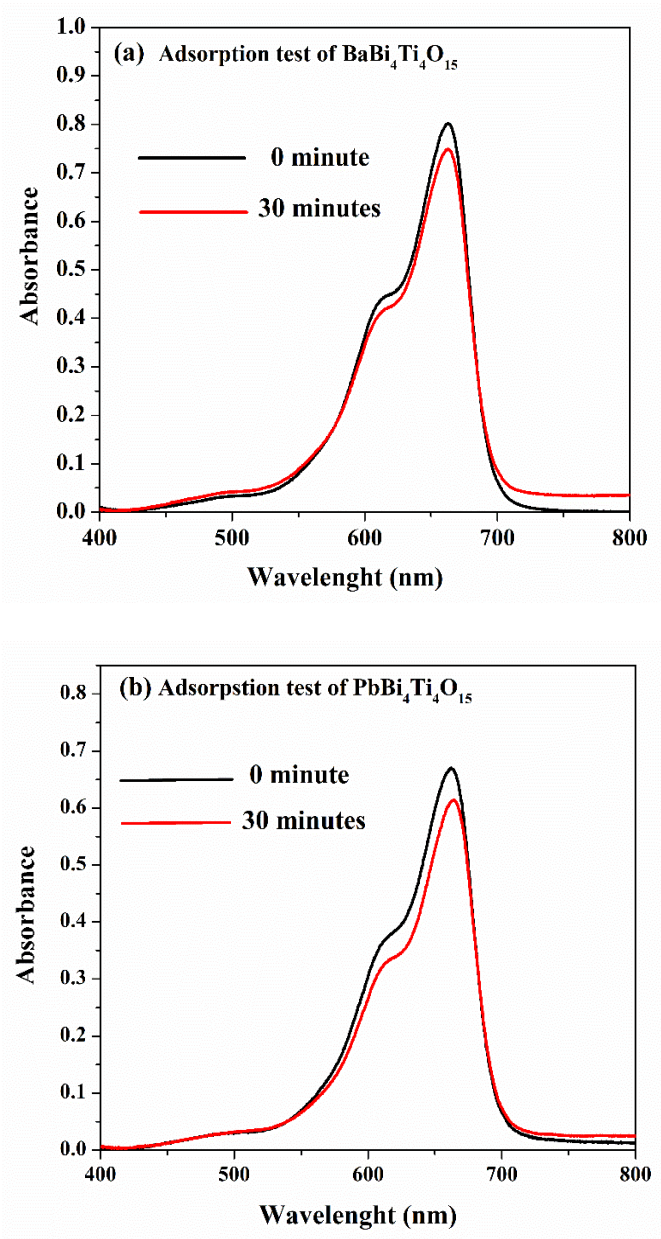

Figure 6. Adsorption test of ABi$_4$Ti$_4$O$_{15}$ (A= Ba, and Pb)

The photocatalytic activity of the ABi$_4$Ti$_4$O$_{15}$ (A= Ba and Pb) compound in reducing the concentration of methylene blue is shown in **Figure 7** and the result was tabulated in **Table 4**. It can be seen that the ABi$_4$Ti$_4$O$_{15}$ (A= Ba, and Pb) compound can decrease the concentration of methylene blue. It indicated that the decrease in methylene blue concentration also occurs through a photocatalysis mechanism. If compared with the adsorption test results for 30-minute, therefore methylene blue concentration decreases by adsorption mechanism is smaller. It showed that the role of the adsorption process in the reduction of methylene blue is minor.

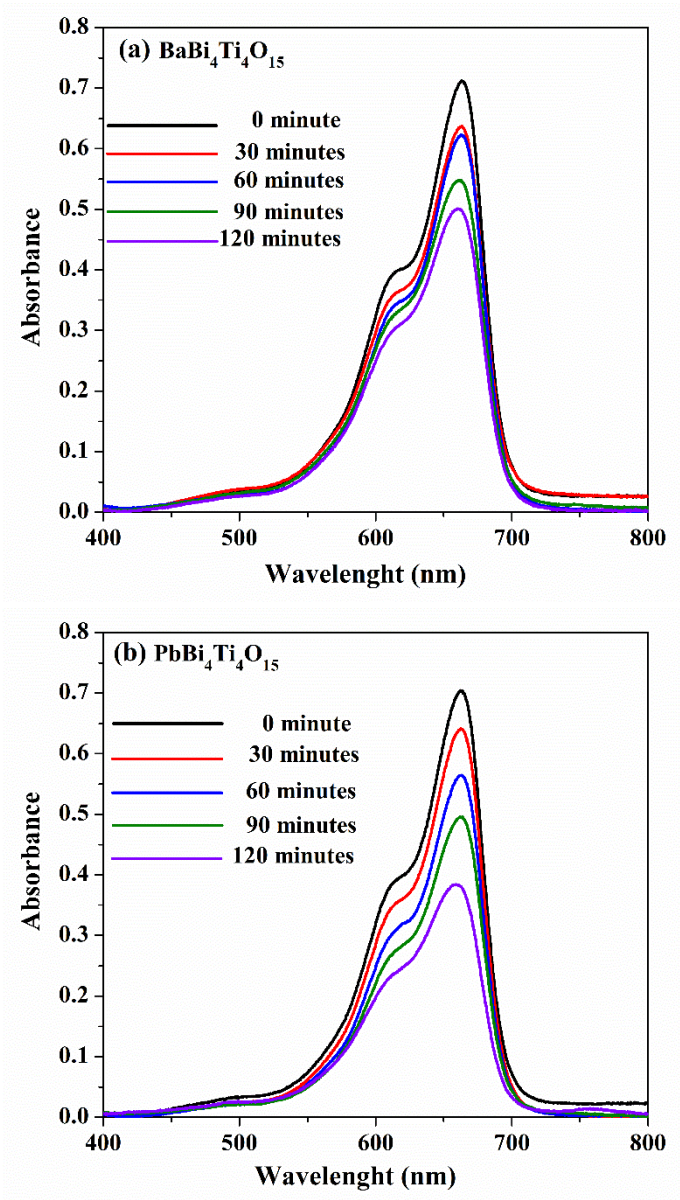

Figure 7. Photocatalyst test of ABi$_4$Ti$_4$O$_{15}$ (A= Ba, and Pb)

Table 4. The photocatalyst test results of ABi$_4$Ti$_4$O$_{15}$ (A= Ba, and Pb)

Compound	Time (minutes)	%Metylene blue concentration decreases
BaBi$_4$Ti$_4$O$_{15}$	30	10.69
	60	12.72
	90	23.70
	120	30.35
PbBi$_4$Ti$_4$O$_{15}$	30	9.33
	60	20.41
	90	30.61
	120	46.65

It is well known that there are two main stages in photocatalysis process, i.e, (1) the adsorption of methylene blue on the surface of the catalyst (ABi$_4$Ti$_4$O$_{15}$ (A= Ba, and Pb)), and then (2) the degradation of methylene blue through a photocatalytic mechanism [46,47]. The degradation of the methylene blue mechanism can be explained as follows: the Bi$_4$Ti$_4$O$_{15}$ photocatalyst material absorbs photon with energy equal to or greater than its band gap energy, which excites e^- from the *VB* to the *CB* and this process creates h^+ in *VB*. The e^- in the *CB* react with O_2 to form •O radicals, while h^+ in the *VB* react with H_2O to produce •OH radicals and can react/degrade methylene blue to CO_2 and H_2O [48]. Table 4 also showed that PbBi$_4$Ti$_4$O$_{15}$ can reduce higher methylene blue concentration, which is likely due to: (1) its lower band gap energy, allowing it to operate across a wider light spectrum, and (2) its higher adsorption ability, resulting in more methylene blue adhering to the catalyst surface and thus more being degraded [49,50]. The degradation yield obtained is still relatively low. This may be due to the relatively high band gap energies of both tested compounds (operating under UV light). Another possible reason is that the particles of both compounds are agglomerated, so the interaction between light and the catalyst particles cannot occur optimally [51].

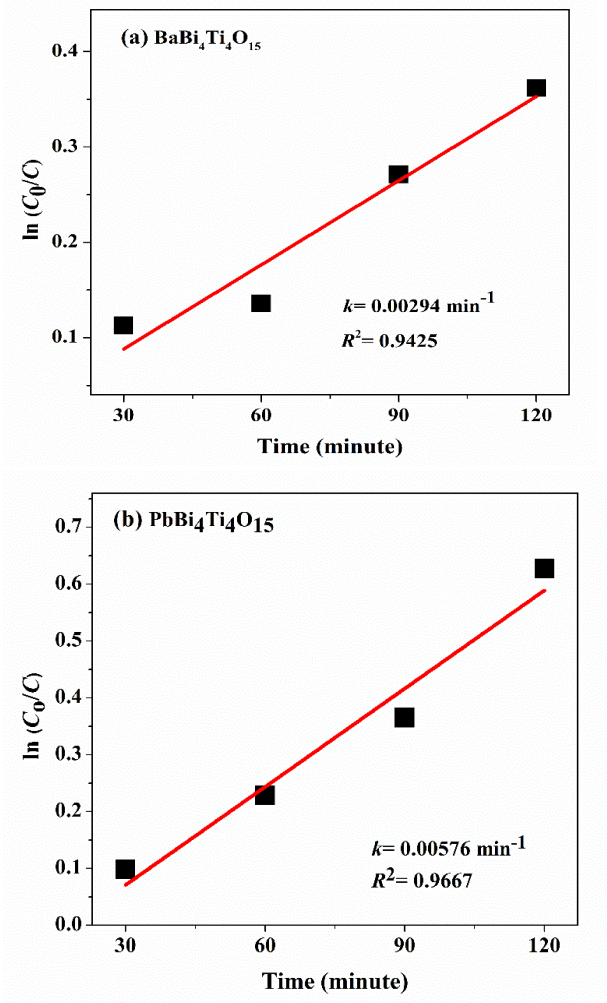

Figure 8. Pseudo first order kinetic plot for the photocatalytic degradation of metylene blue using (a) BaBi$_4$Ti$_4$O$_{15}$, and (b) PbBi$_4$Ti$_4$O$_{15}$.

The degradation kinetics of methylene blue were evaluated using the pseudo first order Langmuir-Hinshelwood model (equation 1) [52].

$$\ln \frac{C_0}{C} = kt \quad (1)$$

With C_0 is the initial concentration of methylene blue, C is the remaining concentration of methylene blue at degradation time (t/minutes), and k is the reaction rate constant. The plot of the pseudo-first-order reaction rate for methylene blue degradation is shown in **Figure 8**. The plotting results give R^2 values for the ABi$_4$Ti$_4$O$_{15}$ compounds (A = Ba, and Pb) of 0.9425 and, 0.9667 respectively. Meanwhile, k were obtained from the slopes, with values of 0.00294 and 0.00567 min^{-1}, respectively. It indicated that the degradation rate of methylene blue by PbBi$_4$Ti$_4$O$_{15}$ is higher than that of BaBi$_4$Ti$_4$O$_{15}$ (it showed by the comparison of the k). And it related to the comparison of the band gap values, where PbBi$_4$Ti$_4$O$_{15}$ has a lower band gap [53].

4. CONCLUSIONS

The plate-like ABi$_4$Ti$_4$O$_{15}$ (A = Ba and Pb) compounds were successfully synthesized via the molten salt method. However, the minor impurities, i.e, (a) BaTiO$_3$ impurity was detected in the BaBi$_4$Ti$_4$O$_{15}$ sample, and (b) Bi$_2$Ti$_2$O$_7$ was detected in the PbBi$_4$Ti$_4$O$_{15}$ sample. The refinement results indicate that differences in the A-site cations in the ABi$_4$Ti$_4$O$_{15}$ compounds (A = Ba, and Pb) affect their structure. The particle morphology of the ABi$_4$Ti$_4$O$_{15}$ (A= Ba and Pb) compounds was found to be plate-like, and agglomeration was still observed. Differences in the type of A-site cation also affect the band gap energy obtained, where PbBi$_4$Ti$_4$O$_{15}$ has a lower band gap energy. This results in a higher capability and faster rate of methylene blue degradation by PbBi$_4$Ti$_4$O$_{15}$.

ACKNOWLEDGMENTS

The author expresses deep gratitude to Department of Chemistry, Faculty Science and Technology, Universitas Islam Negeri Maulana Malik Ibrahim Malang for providing laboratory facilities, which enabled the research to be carried out smoothly.

REFERENCES

1. Oladoye PO, Ajiboye TO, Omotola EO, Oyewola OJ. Methylene blue dye: Toxicity and potential elimination technology from wastewater. *Results Eng*. 2022;16:100678. doi:10.1016/j.rineng.2022.100678
2. Mulushewa Z, Dinbore WT, Ayele Y. Removal of methylene blue from textile waste water using kaolin and zeolite-x synthesized from Ethiopian kaolin. *Environ Anal Heal Toxicol*. 2021;36(1):e2021007-0. doi:10.5620/eaht.2021007
3. Fito J, Abewaa M, Mengistu MA. Adsorption of methylene blue from textile industrial wastewater using activated carbon developed from Rumex abyssinicus. *Sci Rep*. 2023;13:5427. doi:10.1038/s41598-023-32341-w
4. Sitompul DW, Kemala T, Darmawan N. Application of PAN/α-Fe$_2$O$_3$-Bentonite as a photocatalytic membrane for the photodegradation of methylene blue. *J Kim Val*. 2023;9(1):22-29. doi:10.15408/jkv.v9i1.28635
5. Mhaske S, Padwal Y, Chauhan R. Cu-doped TiO$_2$ spheres: enhanced solar-driven photocatalysis for hydrogen generation and degradation of methylene blue and Congo red. *J Mater Sci Mater Electron*. 2024;35:1289. doi:10.1007/s10854-024-13067-5
6. Mohamadpour F, Amani AM. Photocatalytic systems: reactions, mechanism, and applications. *RSC Adv*. 2024;14:20609-20645. doi:10.1039/D4RA03259D
7. Hassaan MA, El-Nemr MA, Elkatory MR. Principles of photocatalysts and their different applications: A Review. *Top Curr Chem*. 2023;381:31. doi:10.1007/s41061-023-00444-7
8. Chakravorty A, Roy S. A review of photocatalysis, basic principles, processes, and materials. *Sustain Chem Environ*. 2024;8:100155. doi:10.1016/j.scenv.2024.100155
9. Malini B, Gandhimathi R. Benefits and challenges of nanotechnology-based photocatalysts in achieving a pollution free environment. *J Environ Anal Chem*. 2025;105(17):5110-5132. doi:10.1080/03067319.2024.2384653
10. Bekele T, Alamnie G. The photocatalytic degradation of organic pollutants-a comprehensive overview. *Results Chem*. 2025;18:102758. doi:10.1016/j.rechem.2025.102758
11. Li Z, Zhu X, Chen Z. Novel Br-doped Bi$_2$WO$_6$ photocatalyst for high-efficiency removal of norfloxacin: mechanism and photocatalytic activity. *Environ Sci Pollut Res*. 2024;31:56210-56226. doi:10.1007/s11356-024-34908-0
12. Halili R, Li Z. Synergizing photocatalysis with Aurivillius-phase Bi$_4$Ti$_3$O$_{12}$: current insights and emerging trends. *J Mater Chem A*. 2025;13:16345-16381. doi:10.1039/D4TA07986H
13. Supriya S. Tailoring layered structure of bismuth-based Aurivillius perovskites: Recent advances and future aspects. *Coord Chem Rev*.

2023;479:215010. doi:10.1016/j.ccr.2022.215010
14. Khan MA, Nadeem MA, Idriss H. Ferroelectric polarization effect on surface chemistry and photo-catalytic activity: A review. *Surf Sci Rep*. 2016;71(1):1-31. doi:10.1016/j.surfrep.2016.01.001
15. Wang Y, Zhang M, Wu J, Hu Z, Zhang H, Yan H. Ferroelectric and photocatalytic properties of Aurivillius phase $Ca_2Bi_4Ti_5O_{18}$. *J Am Ceram Soc*. 2021;104(1):322-328. doi:10.1111/jace.17466
16. He R, Xu D, Cheng B, Yu J, Ho W. Review on nanoscale Bi-based photocatalysts. *Nanoscale Horizons*. 2018;3:464-504. doi:10.1039/C8NH00062J
17. Huang X, Soomro RA, Shen H, Guo L, Yang C, Wang D. Bi_2MO_6 (M = Mo, W) Aurivillius oxides for efficient photocatalytic N_2-to-NH_3 conversion: a perspective review. *Inorg Chem Front*. 2025;12:1773-1797. doi:10.1039/D4QI03182B
18. Kumar A, Sharma P, Wang T, Lai CW, Sharma G, Dhiman P. Recent progresses in improving the photocatalytic potential of $Bi_4Ti_3O_{12}$ as emerging material for environmental and energy applications. *J Ind Eng Chem*. 2024;138:1-16. doi:10.1016/j.jiec.2024.03.054
19. al-Abrar ML, Hastuti E, Prasetyo A. Molten salt synthesis of photocatalyst material $SrBi_4Ti_4O_{15}$ for methylene blue degradation. *J Rekayasa Kim dan Lingkung*. 2023;17(2):182-189. doi:10.23955/rkl.v17i2.25288
20. Febrianti A, Prasetyo A. Ciprofloxacin removal by adsorption photocatalysis effect of $SrBi_4Ti_4O_{15}$. In: *IOP Conference Series: Earth and Environmental Science*. Vol 1574. ; 2025:12006. doi:10.1088/1755-1315/1574/1/012006
21. Qi W, Wang Y, Wu J, Hu Z, Jia C, Zhang H. Relaxor ferroelectric and photocatalytic properties of $BaBi_4Ti_4O_{15}$. *Adv Appl Ceram*. 2019;118(7):418-424. doi:10.1080/17436753.2019.1634943
22. Kumar P, Vaish R, Sung TH, et al. Effect of poling on photocatalysis, piezocatalysis, and photo-piezo catalysis performance of $BaBi_4Ti_4O_{15}$ ceramics. *Glob Challenges*. 2023;7:2200142. doi:10.1002/gch2.202200142
23. Zulhadjri, Prijamboedi B, Nugroho AA, et al. Aurivillius phases of $PbBi_4Ti_4O_{15}$ doped with Mn^{3+} synthesized by molten salt technique: Structure, dielectric, and magnetic properties. *J Solid State Chem*. 2011;184(5):1318-1323. doi:10.1016/j.jssc.2011.03.044
24. Bella I, Wendari TP, Jamarun N, Mufti N, Zulhadjri. Hydrothermal synthesis of $ABi_2Ta_2O_9$ Aurivillius phase: A comparative study of A-site cation size on structure, dielectric, optical properties. *J Adv Dielectr*. 2022;12(2):2150030. doi:10.1142/S2010135X21500302
25. Zhang Z, Yang Y, Wang Y, et al. Revealing the A-site effect of lead-free $A_3Sb_2Br_9$ Perovskite in photocatalytic C(sp^3)-H bond activation. *Angew Chemie*. 2020;132:18293. doi:10.1002/anie.202005495
26. Tian W, Wang R, Yang D. Organic A-cations in metal halide perovskite photovoltaics. *Nat Rev Chem*. 2026;10:50-71. doi:10.1038/s41570-025-00774-8
27. Collu DA, Carucci C, Piludu M, Parsons DF, Salis A. Aurivillius oxides nanosheets-based photocatalysts for efficient oxidation of malachite green dye. *Int J Mol Sci*. 2022;23(10):5422. doi:10.3390/ijms23105422
28. Shetty M, Muniyappa M, Rani MN, Gangaraju V, Shivaramu P, Rangappa D. Photocatalytic efficiency of Bi-based Aurivillius compounds: critical review and discernment of the factors involved. In: Balakumar S, Keller V, Shankar M, eds. *Nanostructured Materials for Environmental Applications*. Cham: Springer; 2021. doi:10.1007/978-3-030-72076-6_6
29. Ozaki D, Suzuki H, Tomita O. A new lead-free Sillén-Aurivillius oxychloride $Bi_5SrTi_3O_{14}Cl$ with triple-perovskite layers for photocatalytic water splitting under visible light. *J Photochem Photobiol A Chem*. 2021;408:113095. doi:10.1016/j.jphotochem.2020.113095
30. Chen Z, Jiang H, Jin W, Shi C. Enhanced photocatalytic performance over $Bi_4Ti_3O_{12}$ nanosheets with controllable size and exposed {001} facets for Rhodamine B degradation. *Appl Catal B Environ*. 2016;180:698-706. doi:10.1016/j.apcatb.2015.07.022
31. Zhao Z, Li X, Ji H, Deng M. Formation mechanism of plate-like $Bi_4Ti_3O_{12}$ particles in molten salt fluxes. *Integr Ferroelectr*. 2014;154(1):154-158. doi:10.1080/10584587.2014.904705
32. Maryani K, Anwari NS, Safitri WN, Hardian A, Inggarwati ED, Prasetyo A. The effect of synthesis temperature on structural, morphological, and band gap energy of plate-like $Bi_4Ti_{2.95}V_{0.05}O_{12}$ prepared by molten NaCl/KCl salt method. *Commun Sci Technol*. 2024;9(1):1-6. doi:10.21924/cst.9.1.2024.1279
33. Wang Z, Wang Z, Feng Y, et al. Plate-like multiprincipal cation ceramic powders with Aurivillius and Perovskite structures fabricated by molten salt synthesis. *Inorg Chem*. 2025;64(23):11721-11730. doi:10.1021/acs.inorgchem.5c01197

34. Nurcahyaningtyas D, Prasetyo A. Synthesis and characterization Fe doped $BaBi_4Ti_4O_{15}$ prepared via molten salt method. In: *AIP Conference Proceedings*. Vol 3106. ; 2024:20005. doi:10.1063/5.0214994
35. Toby BH. R factors in rietveld analysis: How good is good enough? *Powder Diffr*. 2006;21(1):67-70. doi:10.1154/1.2179804
36. García-Guaderrama M, Fuentes L, Márquez-Lucero A, Blanco O. Structural stability and cation disorder in Aurivillius phases. *Mater Res Bull*. 2012;47(11):3850-3854. doi:10.1016/j.materresbull.2012.08.038
37. Hervoches CH, Lightfoot P. Cation Disorder in Three-Layer Aurivillius Phases: Structural Studies of $Bi_{2-x}Sr_{2+x}Ti_{1-x}Nb_{2+x}O_{12}$ ($0<x<0.8$) and $Bi_{4-x}La_xTi_3O_{12}$ (x=1 and 2). *J Solid State Chem*. 2000;153(1):66-73. doi:10.1006/jssc.2000.8741
38. Prasetyo A, Guntur ANM, Himmah SN, Aini N, Rouf UA, Aziz A. Synthesis of microsheets $Bi_4Ti_3O_{12}$, and $Bi_4Ti_{2.95}V_{0.05}O_{12}$ via molten NaCl-KCl salt method. *J Pure Appl Chem Res*. 2022;11(3):207-213. doi:10.21776/ub.jpacr.2022.011.03.703
39. Garcia MAP, Gupta SK, Mao Y. Effects of molten-salt processing parameters on the structural and optical properties of preformed $La_2Zr_2O_7$: Eu^{3+} nanoparticles. *Ceram Int*. 2020;46(2):1352-1361. doi:10.1016/j.ceramint.2019.09.098
40. Zuniga JP, Abdou M, Gupta SK, Mao Y. Molten-salt synthesis of complex metal oxide nanoparticles. *J Vis Exp*. 2018;140:58482. doi:10.3791/58482
41. Marela SD, Aini N, Hardian A, Suendo V, Prasetyo A. The effect of synthesis temperature on the plate-like particle of $Bi_4Ti_3O_{12}$ obtained by molten NaCl salt method. *J Pure Appl Chem Res*. 2021;10(1):64-71. doi:10.21776/ub.jpacr.2021.010.01.570
42. Hur SG, Kim TW, Hwang SJ, Choy JH. Influences of *A*- and *B*-site cations on the physicochemical properties of Perovskite-structured $A(In_{1/3}Nb_{1/3}B_{1/3})O_3$ (*A*= Sr, Ba; *B*= Sn, Pb) photocatalysts. *J Photochem Photobiol A Chem*. 2006;183(1-2):176-181. doi:10.1016/j.jphotochem.2006.03.014
43. Cahyo IN, Aini N, Steky F V, Suendo V, Safitri WN, Prasetyo A. Synthesis of plate-like Fe-doped $SrBi_4Ti_4O_{15}$ using Na_2SO_4/K_2SO_4 molten salt method: XRD, Raman spectroscopy, SEM, and Uv-Vis DRS studies. *J Iran Chem Soc*. 2023;20:3079-3085. doi:10.1007/s13738-023-02899-3
44. Banerjee S, Debnath A, Allam BK, Musa N. Adsorptive and photocatalytic performance of perovskite material for the removal of food dye in an aqueous solution. *Environ Challenges*. 2021;5:100240. doi:10.1016/j.envc.2021.100240
45. Huang L, Huang X, Yan J. Research progresses on the application of perovskite in adsorption and photocatalytic removal of water pollutants. *J Hazard Mater*. 2023;442:130024. doi:10.1016/j.jhazmat.2022.130024
46. Kusiak-Nejman E, Sienkiewicz A, Wanag A, Rokicka-Konieczna P, Morawski AW. The role of adsorption in the photocatalytic decomposition of dyes on APTES-modified TiO2 nanomaterials. *Catalysts*. 2021;11(2):172. doi:10.3390/catal11020172
47. Bekhit SM, Zaki SA, Hassouna MSD. Combined effect of adsorption and photocatalytic degradation using magnesium oxide nano-flowers for tetracycline removal. *J Inorg Organomet Polym Mater*. 2024;34:5006-5019. doi:10.1007/s10904-024-03138-9
48. Kalaycıoğlu Z, Özuğur U, Bengü P, Önder E, Erim FB. Efficient photocatalytic degradation of methylene blue dye from aqueous solution with cerium oxide nanoparticles and graphene oxide-doped polyacrylamide. *ACS Omega*. 2023;8(14):13004-13015. doi:10.1021/acsomega.3c00198
49. Kumar A, Pandey G. A review on the factors affecting the photocatalytic degradation of hazardous materials. *Mater Sci Eng Int J*. 2017;1(3):106-114. doi:10.15406/mseij.2017.01.00018
50. Li X, Chen Y, Tao Y, et al. Challenges of photocatalysis and their coping strategies. *Chem Catal*. 2022;2(6):1315-1345. doi:10.1016/j.checat.2022.04.007
51. Pellegrino F, Pellutiè L, Sordello F. Influence of agglomeration and aggregation on the photocatalytic activity of TiO_2 nanoparticles. *Appl Catal B Environ*. 2017;216:80-87. doi:10.1016/j.apcatb.2017.05.046
52. Tran HD, Nguyen DQ, Do PT, Tran UNP. Kinetics of photocatalytic degradation of organic compounds: a mini-review and new approach. *RSC Adv*. 2023;13:16915-16925. doi:10.1039/D3RA01970E
53. Naseri A, Samadi M, Mahmoodi NM, Pourjavadi A, Mehdipour H, Moshfegh AZ. Tuning composition of electrospun ZnO/CuO nanofibers: toward controllable and efficient solar photocatalytic degradation of organic pollutants. *J Phys Chem C*. 2017;121(6):3327-3338. doi:10.1021/acs.jpcc.6b10414